Free Surface Model to Predict the Influence of Shrinkage Cavities on the Solute Redistribution in Castings

G. Ehlen, A. Schweizer, A. Ludwig, P.R. Sahm
Foundry Institute, RWTH-Aachen
Intzestr. 5, D-52056 Aachen, Germany

Abstract

The final distribution of macrosegregations in castings is strongly influenced by the solidification behavior and the movement of the melt surface. The last point to solidify is identical to the area of the maximally enriched melt. The present work uses a 2D control-volume-method (CVM) model based on volume-averaging to predict the transient shape of the surface and the shrinkage cavity as well as their influence on the final solute distribution. The solute transport mechanisms are feeding flow, thermo-solutal convection and macroscopic diffusion in the liquid. Mushy zone flow is described by an anisotropic permeability model. The moving surface is realized by implementing a volume-of-fluid model. Phase transitions are calculated using nonlinear eutectic or peritectic phase diagrams taking into account one liquid and two solid phases.

Modeling of Casting, Welding and Advanced Solidification Processes IX
Edited by Peter R. Sahm, Preben N. Hansen and James G. Conley

1. Introduction

The final distribution of macrosegregations in castings is strongly influenced by the solidification behavior and the movement of the melt surface. The last point to solidify is identical to the area of the maximally enriched melt. In the present work a numerical model is presented that can predict the movement of the melt surface during solidification as well as the final shape and position of the shrinkage cavity. The numerical results are compared to an experimentally observed shrinkage cavity.

2. Numerical Procedure

The present approach uses a 2D control-volume-method (CVM) volume-averaging model for one liquid and two stationary solid phases (liquid: *l*, solid-delta: δ, solid-gamma: γ). The following conservation equations are solved: mixture enthalpy, x- and y-momentum for *l*, mass, species for *l*,. The cosrresponding equations are:

$$\frac{\partial}{\partial t}(\varepsilon_l \rho_l) + \bar{\nabla}(\varepsilon_l \rho_l \bar{v}_l) = -\Gamma_{\delta l} - \Gamma_{\gamma l} \tag{1a}$$

$$\frac{\partial}{\partial t}(\varepsilon_\delta \rho_\delta) = \Gamma_{\delta l} \quad \text{and} \quad \frac{\partial}{\partial t}(\varepsilon_\gamma \rho_\gamma) = \Gamma_{\gamma l} \tag{1b}$$

$$\frac{\partial}{\partial t}(\varepsilon_l \rho_l \vec{v}_l) + \bar{\nabla}(\varepsilon_l \rho_l \bar{v}_l \otimes \bar{v}_l) = -\varepsilon_l \bar{\nabla} p + \bar{\nabla}\bar{\bar{\tau}}_l + \varepsilon_l \rho_l \vec{g} + \vec{M}_l^{\Gamma} + \vec{M}_l^{d} \tag{2a}$$

$$\text{with} \quad \bar{\bar{\tau}}_l = \mu_l \left\{ \bar{\nabla}(\varepsilon_l \bar{v}_l) + \left[\bar{\nabla}(\varepsilon_l \bar{v}_l)\right]^T \right\} \tag{2b}$$

$$\frac{\partial}{\partial t}(\varepsilon_l \rho_l C_l) + \bar{\nabla}(\varepsilon_l \rho_l \bar{v} C_l) = \bar{\nabla}(\varepsilon_l \rho_l D_l \bar{\nabla} C_l) + J_l^{\Gamma} \tag{3}$$

$$\frac{\partial}{\partial t}(\varepsilon_l \rho_l h_l + \varepsilon_\delta \rho_\delta h_\delta + \varepsilon_\gamma \rho_\gamma h_\gamma) + \bar{\nabla}(\varepsilon_l \rho_l \bar{v} h_l) = -\bar{\nabla}\vec{q}_{l+\delta+\gamma} + S_{l+\delta+\gamma} \tag{4}$$

where $\varepsilon_l, \varepsilon_\delta, \varepsilon_\gamma$ are the volume fractions, $\rho_l, \rho_\delta, \rho_\gamma$ the densities and h_l, h_δ, h_γ the enthalpies of the three phases. $\bar{v}_l$ is the velocity, μ_l the viscosity, and $\bar{\bar{\tau}}_l$ the strain tensor of the liquid. $\vec{g}$ is the gravitational acceleration and p the pressure. The volume-averaging method follows J. Ni and C. Beckermann [1]. The system of nonlinear differential equations has been discretized in an implicit formulation and is solved using the SIMPLER algorithm by S.V. Patankar [2]. Further details about the source and exchange terms are given in the following section.

2.1 Source and Exchange Terms

Heat of Fusion

The source term for the mixture enthalpy conservation equation arises from the enthalpy difference of liquid and delta (heat of fusion for delta formation) and liquid and gamma (heat of fusion for gamma formation):

$$S_{l+\delta+\gamma} = (h_l - h_\delta)\Gamma_{\delta l} + (h_l - h_\gamma)\Gamma_{\gamma l} \tag{5}$$

Species Transfer

It is assumed that during each time step the solid phase grows by adding a thin solid shell (not necessarily uniform in thickness) from the melt. The corresponding decrease of the liquid mass per volume and time is simply Γ_{sl} (for $s = \delta, \gamma$). Therefore the mass of the species in the liquid per vol-

ume and time is reduced by $C_l\Gamma_{sl}$. From this mass of the species $k_s C_l \Gamma_{sl}$ is incorporated in the solid (k_s is the equilibrium distribution coefficient of the species in s). Thus the reduction of liquid mass of the species by $C_l\Gamma_{sl}$ is partly compensated by the amount $(1-k_s)C_l\Gamma_{sl}$ which represents the mass of species not incorporated into the solid shell. In conclusion the source term of the conservation equation of liquid species mass fraction is chosen to be

$$J_l^{\Gamma} = -k_\delta C_l \Gamma_{\delta l} - k_\gamma C_l \Gamma_{\gamma l} \tag{6}$$

The concentration in delta and gamma is assumed to be simply $C_\delta = k_\delta C_l$ and $C_\gamma = k_\gamma C_l$. Thus, no back-diffusion model is applied in this work. The resulting macrosegregation is described by

$$C_{mix} = \frac{\varepsilon_l \rho_l C_l + \varepsilon_\delta \rho_\delta C_\delta + \varepsilon_\gamma \rho_\gamma C_\gamma}{\varepsilon_l \rho_l + \varepsilon_\delta \rho_\delta + \varepsilon_\gamma \rho_\gamma}. \tag{7}$$

Mass Transfer

The mass transfer from the liquid to delta and/or gamma is determined in an iterative way by accounting for the validity of the phase diagram. For this purpose the phase diagram is considered as peace-wise linear. The discretized enthalpy equation and liquid species conservation equation can be written as $T = T(\varepsilon_s)$ and $C_l = C_l(\varepsilon_s)$. The phase diagram yields the third equation needed to calculate T, C_l and ε_S: $T = T_{liq}(C_l)$. This scheme works for the case of primary δ- or γ-solidification. For the eutectic or peritectic solidification we have $T = T(\varepsilon_\delta, \varepsilon_\gamma)$ and $C_l = C_l(\varepsilon_\delta, \varepsilon_\gamma)$. The conditions at the eutectic/peritectic plateau yield the fourth equation to solve for the fourth variable: $C_l = C_{eut\,l\,per}$ or $T = T_{eut\,l\,per}$. The solution of this set of three or four equations is done using a Newton-Raphson iteration scheme.

Momentum Transfer

The choice of adequate momentum exchange terms between the dendritic network and the flowing melt is subject of ongoing scientific discussions. In this work the following approach for the momentum transfer due to the phase change is used:

$$\bar{M}_l^{\Gamma} = -\vec{v}\left[\frac{\partial}{\partial t}(\varepsilon_\delta \rho_\delta) + \frac{\partial}{\partial t}(\varepsilon_\gamma \rho_\gamma)\right] \tag{8}$$

For the considered case of stationary solid phase this term is different for solidification and remelting. Solidifying mass that settles down to the stationary solid is stopped and its momentum gets lost. This does not alter the velocity of the fluid. Remelting solid has to be accelerated to the average velocity in the cell. In this case the velocity of the fluid decreases.

The momentum loss of the melt inside of the mushy zone due to friction can be described using a Darcy term [3]:

$$\bar{M}_l^{d} = -\varepsilon_l^2 \mu_l K^{(2)-1} \bar{v} \tag{9a}$$

$$\text{with} \quad K^{(2)-1} = \begin{bmatrix} \frac{\cos^2\varphi}{K_{\xi\xi}} + \frac{\sin^2\varphi}{K_{\eta\eta}} & \sin\varphi\cos\varphi\left(\frac{1}{K_{\xi\xi}} - \frac{1}{K_{\eta\eta}}\right) \\ \sin\varphi\cos\varphi\left(\frac{1}{K_{\xi\xi}} - \frac{1}{K_{\eta\eta}}\right) & \frac{\sin^2\varphi}{K_{\xi\xi}} + \frac{\cos^2\varphi}{K_{\eta\eta}} \end{bmatrix} \tag{9b}$$

$K_{\xi\xi}$ and $K_{\eta\eta}$ are the permeabilities parallel and normal to the primary dendrite arms and φ is the angle between the primary dendrite arms and the x-axis. For columnar dendritic solidification the direction denoted by φ points along the temperature gradient.

In the case of isotropic permeability of the mushy zone using a Blake-Kozeny model $K^{(2)}$ reduces to

$$K = K_0 \frac{\varepsilon_l^3}{(1-\varepsilon_l)^2} \quad \Rightarrow \quad \bar{M}_l^d = -\frac{\mu_l}{K_0}\frac{(1-\varepsilon_l)^2}{\varepsilon_l}\bar{v} \tag{9c}$$

This model was used for the presented calculation.

2.2 Free Surface Model

To describe shrinkage effects due to phase change and temperature dependent densities a moving free surface was implemented using a volume of fluid (VOF) model that is based on the one presented by B.D. Nichols *et al.* [4]. The governing equation for the VOF-function F is:

$$\frac{\partial F}{\partial t} + u\frac{\partial F}{\partial x} + v\frac{\partial F}{\partial y} = 0 \tag{10}$$

To apply this equation to cases with non constant densities and non constant phase fractions the classical donor-acceptor flux approximation had to be modified mainly in three points:

- The velocities u and v had to become superficial velocities u_s and v_s instead of pore velocities u_p and v_p. In the case of partially solidified cells the relations $u_s = \varepsilon_l u_p$ and $v_s = \varepsilon_l v_p$ hold, where ε_l denotes the liquid fraction at the corresponding cell boundaries. The use of superficial velocities makes the velocity of the moving surface depend on the volume of the transported liquid and not on the "real" velocities inside the dendritic network.

- The time dependent term had to be extended by a term taking into account the VOF appearing or disappearing by phase change and shrinkage (index ^{0} denotes values of old time step):

$$\Delta F = \frac{\varepsilon_l^0\rho_l^0 + \varepsilon_\delta^0\rho_\delta^0 + \varepsilon_\gamma^0\rho_\gamma^0}{\varepsilon_l\rho_l + \varepsilon_\delta\rho_\delta + \varepsilon_\gamma\rho_\gamma} - 1 \tag{11}$$

- The free surface boundary condition had to be adapted. In cells containing a part of the free surface the continuity equation must be fulfilled. The original VOF-model accounts for this condition by driving the velocity divergence inside the surface cells to zero. Considering inhomogeneous and transient density and phase fraction distributions the complete discretized continuity equation

$$\begin{aligned} &(\varepsilon_l\rho_l - \varepsilon_l^0\rho_l^0 + \varepsilon_\delta\rho_\delta - \varepsilon_\delta^0\rho_\delta^0 + \varepsilon_\gamma\rho_\gamma - \varepsilon_\gamma^0\rho_\gamma^0)\Delta x\Delta y + \\ &((\varepsilon_l\rho_l)_{east}v_{east} - (\varepsilon_l\rho_l)_{west}v_{west})\Delta y\Delta t + ((\varepsilon_l\rho_l)_{north}v_{north} - (\varepsilon_l\rho_l)_{south}v_{south})\Delta x\Delta t = 0 \end{aligned} \tag{12}$$

must be used to set the boundary velocities in the surface cells.

For most differential equations the densities of the alloy elements are assumed to be equal to the density of the matrix. The only exception are the buoyancy terms of the momentum conservation equation that are used to model solutal convection.

3. Experimental and numerical work

For validating the model a cylindrical Al7wt%Si ingot (H = 107 mm, R = 40 mm) was cast in a cast iron chill which stood freely on a steel plate, Fig. 1a). The temperature in the furnace before casting was 990 K. Fig. 2e) shows the resulting surface geometry after total solidification. Below the middle of the shrinkage cavity there are two hot cracks and an area of shrinkage porosities that are not considered in the actual numerical model. The cavity in the middle of the block is due to gas formation at one of the thermocouples.

The numerical model was applied to this casting process. Fig. 1b) shows the calculation grid and the boundary conditions. The time dependent temperature boundary conditions at the contact zone between casting and chill were taken from a MAGMAsoft™ solidification calculation (without mold filling). The heat transfer coefficients for the MAGMAsoft™ calculation were adapted to a total solidification time similar to the one that was experimentally observed. The initial temperature was set to 900 K, taking into account the heat loss of the alloy on its way from the furnace to the chill and during the mold filling. The time stepwidth was fix and set to 0.1 s with a total solidification time of 120 s. The calculation took about 24 hours using an R10000 Processor. So in the present state the usage of a much finer grid is not reasonable.

Table 1 shows the calculation parameters for the AlSi alloy system. The parameters were determined by comparing material data for different AlSi alloys from different sources.

Table 1: Calculation parameters

liquid density	ρ_l = 2400 kg/m^3	• moving free surfaces • shrinkage induced flow (caused by phase transition) • mushy zone flow • convective solute transport
solid density	ρ_s = 2600 kg/m^3	
liquid heat capacity	$C_{p,l}$ = 1126 W/(kg·K)	
solid heat capacity	$C_{p,s}$ = 1137 W/(kg·K)	
liquid conductivity	λ_l = 75 W/(m·K)	
solid conductivity	λ_s = 165 W/(m·K)	
dynamic viscosity	$\mu = 1.125 \cdot 10^{-2}$ kg/(m·s)	
permeability constant	$K_o = 8 \cdot 10^{-11}$	

4. Results and Discussion

In order to test the shrinkage and free surface algorithm, thermosolutal convection, temperature dependent liquid density and macroscopic diffusion in the liquid had been ommitted in the first simulations presented here (Fig. 2). The calculation results show the typical behavior of an alloy with long freezing range. The mushy zone grows quickly and fills the whole casting after 60 s. After 80 s the shrinkage cavity at the free surface is fully developed and the calculated shape shows a promising agreement with the experimental results, Fig. 2e). The surface slope depends on the remaining surface area open to the liquid. With beginning solidification the open surface area is reduced and the sinking velocity of the surface is increased. This mechanism results in a flat outer area and a steep slope in the center. These characteristics of the real casting are reproduced by the simulation very well.

The time evolution of the solute redistribution shows interesting effects. After 10 s a small part in the bottom edge is completely solid. The solid cells are slightly enriched. A certain area of the mushy zone in front of the solidified cells is slightly depleted. This effect of inverse segregation is caused by the shrinkage induced flow. Principally the initial concentration C_0 (mass fraction) inside a cell is not changed by density changes. If a cell contracts, the mass proportions remain the same. But if a constant volume is considered (cells in a rigid grid), the volume deficit has to be compensated by a flux from the neighbor cells. In the considered case the neighbor cells are partially solidified and thus contain (in the lever-rule model) enriched liquid of concentration $C_l > C_0$. Thus the cell gains enriched liquid and will also be enriched after total solidification. In the neighbor cells the inverse mechanism works: They loose highly enriched liquid and gain liquid from cells that have a smaller solid fraction and thus a smaller liquid concentration down to C_0. With proceeding solidification the completely solidified cells get less enriched. The quantitative correctness of the predicted macrosegregations has to be tested. The impact of thermosolutal convection, temperature dependent liquid densitiy and macroscopic diffusion in the liquid on the shrinkage cavity and the segregations is subject of a subsequent paper.

5. Conclusions and Outlook

The main conclusions of this work are:

- A numerical model was presented, that can describe the movement of the melt surface during the solidification of alloys with binary eutectic phase diagrams.
- The calculated surface shape of the shrinkage cavity on a cylindrical Al7wt%Si ingot shows a promising agreement with experimental results.
- The model for convective solute transport considering mushy zone flow predicts inverse segregations.

The main future tasks will consist in the following:

- Modeling the mass balance inside the surface cells. When a stable dendritic network has formed at the surface, the shrinkage flow causes a porous surface layer. This process, that can be observed on the surface of solidifying ingots is restricted and stopped by capillary forces,
- Modeling outflow and solidification in a single surface cell at the same time,
- Refining free surface boundary conditions for concentrations, phase fractions and pressure,
- Developing different mushy zone and surface models for planar and dendritic solidification,
- Parallelizing the software code to make the use of a much finer grid possible.

Acknowledgement

This research was sponsored by the German Science Foundation DFG under Sa 335/30 for which the authors wish to express their gratitude.

References

[1] J. Ni, and C. Beckermann, "A Volume Averaged Two-Phase Model for Transport Phenomena during Solidification", Metall. Trans. B 22, pp 349-361 (1991).

[2] M. C. Schneider, and C. Beckermann, "Summary of a method for numerically simulating the columnar dendritic solidification of binary alloys", Report UIME-CB01-1993, Dept. of Mechanical Engineering, The University of Iowa, Iowa City, (1993).

[3] Suhas V. Patankar, "Numerical Heat Transfer and Fluid Flow", New York, NY: Hemisphere Publishing Corporation, (1980).

[4] B.D. Nichols, C.W. Hirt, and R.S. Hotchkiss, "SOLA-VOF: A Solution Algorithm Transient Fluid Flow with Multiple Free Boundaries", Los Alamos, University of California (1980).

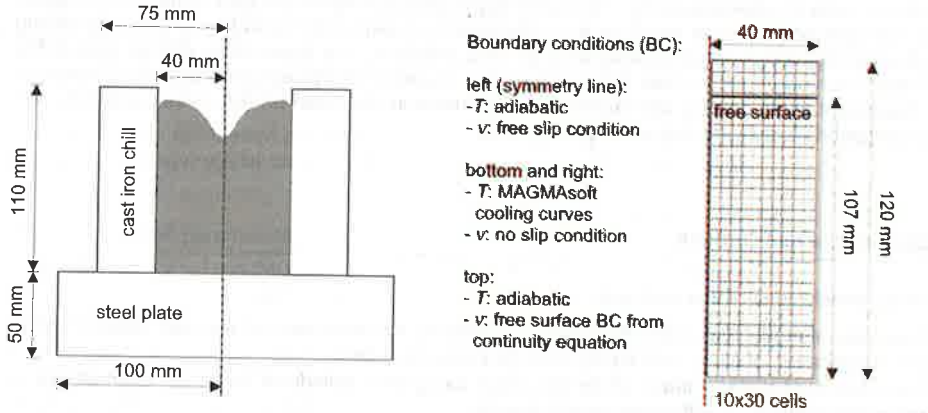

Figure 1a) Experimental setup for the casting of a cylindrical Al7wt%Si ingot. b) Corresponding calculation domain and boundary conditions for the numerical simulation.

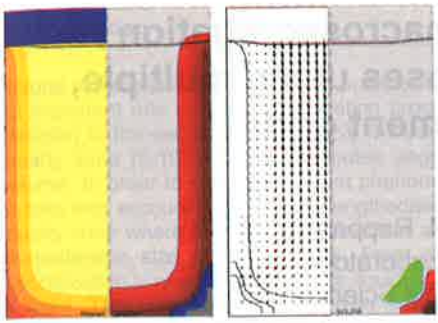

Figure 2a) Distribution of temperature T, solid fraction ε_s, velocities and Si-concentration after 10 s

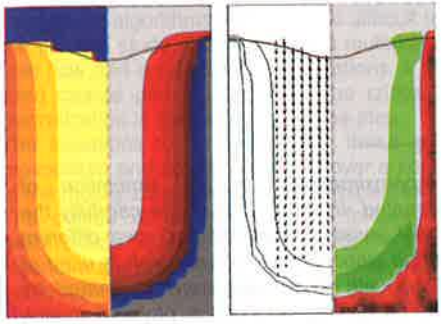

Figure 2b) Distribution of temperature, solid fraction ε_s, velocities and Si-concentration after 30 s

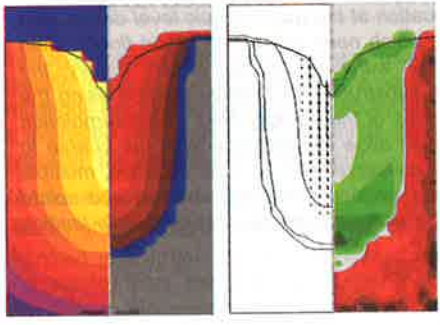

Figure 2c) Distribution of temperature, solid fraction ε_s, velocities and Si-concentration after 60 s

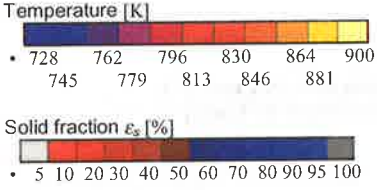

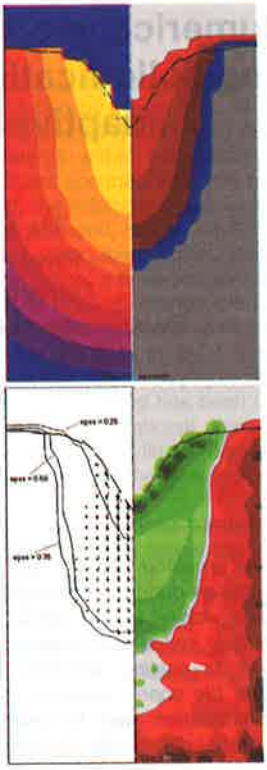

Figure 2d) Distribution of temperature, solid fraction ε_s, velocities and Si-concentration after 80 s

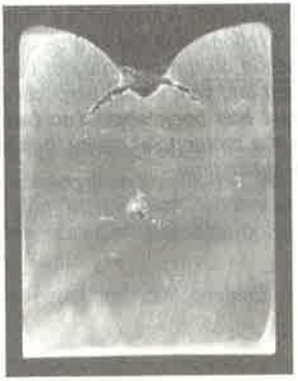

Figure 2e) Experiment: Cross section of the cylindrical Al7wt%Si ingot with shrinkage cavity

v_{max} (t = 60 s) = 0,0025 m/s